# Neutron and Photon Emission from Dysprosium and Terbium Compound Nuclei: Range Distributions*

JOHN M. ALEXANDER†
*State University of New York at Stony Brook, Stony Brook, New York, and Lawrence Radiation Laboratory, University of California, Berkeley, California*

AND

JACOB GILAT AND DAVID H. SISSON‡
*Lawrence Radiation Laboratory, University of California, Berkeley, California*

(Received 14 May 1964)

Electrostatic collection of Tb and Dy recoils stopped in $H_2$ gas has been explored and found satisfactory for the study of recoil-range distributions. For the reactions $Pr^{141}(C^{12},4n)Tb^{149g}$, $Nd^{146}(B^{11},8n)Tb^{149g}$, $Nd^{144}(C^{12},xn)Dy^{156-x}$, and $Ce^{140}(O^{16},xn)Dy^{156-x}$ (where $x=5$, 6, or 7), the range distributions are determined by the initial velocity distributions of the recoiling reaction products. The comparison of previously measured angular distributions with these range distributions provides a good method of determining average total neutron energies. The method is relatively insensitive to angular anisotropies $[d\sigma(0°)-d\sigma(90°)]/d\sigma(90°)$ of less than about unity, but can provide clear evidence for strong forward-backward peaking in the angular distribution of the neutrons. The results are consistent with nearly isotropic neutron emission for the latter two reactions, and previously reported neutron energies are supported. Strong forward-backward peaking of the neutrons is indicated for the former two reactions and previously reported neutron energies are corrected by about 20%.

## I. INTRODUCTION

THIS paper is one of a series that explores the properties of compound nuclei of energy up to 120 MeV and angular momentum up to $100\hbar$. In previous studies measurements were made of the formation cross sections, recoil ranges, and angular distributions of Dy and Tb nuclides produced in heavy-ion-induced reactions. The average range values give strong but indirect evidence for neutron emission essentially symmetric about 90 deg in the c.m. system.[1] Also, the excitation functions exhibit a clear regularity and depend on the average angular momenta of the compound systems.[2] These observations are interpreted as evidence for the applicability of the compound nucleus and statistical models to these reactions.

The average total energies of the emitted neutrons and photons were obtained from an analysis of the angular distributions of these Dy and Tb products.[3] In this analysis, isotropic neutron emission was assumed. It was pointed out that the assumption of isotropy could be tested by measuring the range straggling of the products due to their distribution of velocities. The range straggling in aluminum foils was found to result primarily from the stopping process and from inhomogeneities of the foils.[1]

This report deals with the electrostatic collection of Dy and Tb recoils stopped in hydrogen gas and discusses the use of this technique to determine range distributions. Theoretical considerations and various tests of the collection method indicate that the range distributions thus obtained are primarily due to the velocity distributions of the products. The comparison of these range distributions with the angular distributions verifies the approximation of isotropic neutron emission for the reactions $Nd^{144}(C^{12},5n)Dy^{151}$; $Nd^{144}(C^{12},6n)Dy^{150}$; $Nd^{144}(C^{12},7n)Dy^{149}$; $Ce^{140}(O^{16},5n)Dy^{151}$; $Ce^{140}(O^{16},6n)Dy^{150}$; and $Ce^{140}(O^{16},7n)Dy^{149}$; for these reactions the previously reported[3] values of average total neutron and photon energies ($T_n$ and $T_\gamma$) are confirmed. A rather pronounced forward-backward peaking is indicated for neutron emission in the reactions $Nd^{146}(B^{11},8n)Tb^{149g}$ and $Pr^{141}(C^{12},4n)Tb^{149g}$, and corrected values for the neutron and photon energies ($T_n$ and $T_\gamma$) are derived from the data by an approximate method.

## II. EXPERIMENTAL METHOD

### A. Apparatus and Typical Experimental Conditions

We have studied Dy and Tb recoils from reactions of heavy ions ($B^{11}$, $C^{12}$, $O^{16}$, and $Ne^{20}$) with various targets made of thin layers of the appropriate separated isotopes evaporated onto Al backing 0.00025 in. thick. The recoils are initially directed in a narrow cone along the beam direction (<15 deg).[3] They are slowed down in $H_2$ gas and collected on two parallel plates covered with Al foil which are maintained at a potential difference from 500 to 2000 V. The spatial distribution of the radioactive products is determined by cutting the collector foil into strips, which are assayed for $\alpha$ activity as previously described.[1–3] A schematic diagram of the

* Work performed under the auspices of U. S. Atomic Energy Commission.

† Present address: State University of New York at Stony Brook, Stony Brook, Long Island, New York.

‡ International Atomic Energy Agency Fellow from the Israel Atomic Energy Commission, Soreq Research Establishment, Yavneh, Israel.

[1] J. M. Alexander and D. H. Sisson, Phys. Rev. **128**, 2288 (1962).

[2] J. M. Alexander and G. N. Simonoff, Phys. Rev. **133**, B93 (1964).

[3] G. N. Simonoff and J. M. Alexander, Phys. Rev. **133**, B104 (1964).

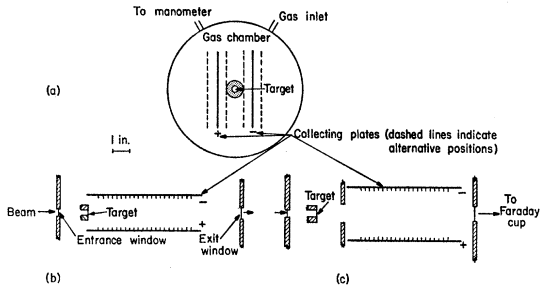


FIG. 1. Schematic diagram of recoil collection apparatus, showing the various collector positions: (a) front view; (b) top view, normal collector position; (c) top view, recessed collector position.

apparatus is shown in Fig. 1. The beam enters the gas-tight chamber through a 0.001-in. Dural window and passes through two 3/8-in. collimators, spaced about 3 in. apart. The second collimator also serves as target mount. Energy-degrading aluminum foils, when used, are mounted on the first collimator. After passing through the target, the beam is monitored by a Faraday cup, separated from the chamber by a second window. This gas-stopping technique has been used previously by several other workers.[4–6]

The chamber and U-tube mercury manometer were flushed several times with hydrogen gas before each exposure. The chamber was then filled to the desired pressure and sealed. Opposite potentials, usually 1000 V with respect to the grounded target mount and chamber walls, were applied to the collector plates. Pressure readings were taken before and after each exposure; the final pressure was never more than 0.05 in. greater than the initial pressure and a difference of 0.02 in. was typical.

Most of the recoil collection (40 to 70%) was on the negative plate. The positive plate collected about one-tenth as much as the negative. The lack of reproducibility of the collection efficiency is attributed to variable levels of impurities in the gas. There was no detectable dependence of collection efficiency on voltage, but it seemed to be lowered by increasing gas pressure.

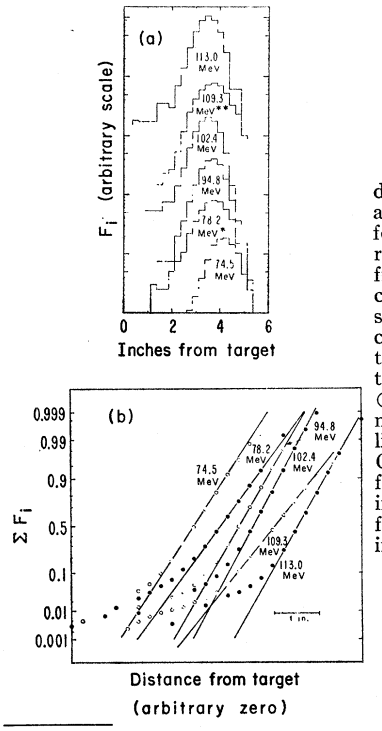


FIG. 2. (a) Range distribution histograms and (b) probability plots for $Nd^{144}(C^{12},xn)Dy^{149-151}$ reactions. $F_i$ denotes the fraction of total activity collected on the $i$th $\frac{1}{4}$-in. strip. $\Sigma F_i$ denotes the cumulative fraction of total activity collected through the $i$th strip. ○, ● indicate experimental points; solid lines show the best Gaussian fit. *: 0.5 in. further from target than indicated. **: 1.0 in. further from target than indicated.

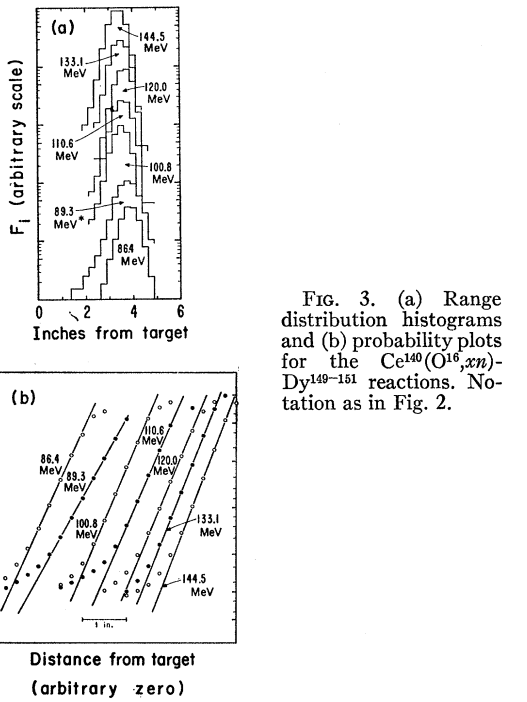


FIG. 3. (a) Range distribution histograms and (b) probability plots for the $Ce^{140}(O^{16},xn)$-$Dy^{149-151}$ reactions. Notation as in Fig. 2.

The Hilac furnishes 3-msec beam pulses at a frequency of 10 to 15 pulses/sec. Exposure to average beam current greater than 75 m$\mu$A gave rise to an upward drifting of the collected recoils. The drift distance increased with increasing beam intensity and is presumed to be due to convection currents. If the ions move toward the plates with a mean velocity of $\approx 10^4$ cm/sec (as discussed in Sec. II.B), then convection currents of $\approx 10^3$ cm/sec or $\approx 20$ mph would cause detectable upward drifts. The width of the range distributions in the beam direction was not appreciably affected by even the largest upward drift observed ($\approx 1/4$ in.). Experiments were performed at low beam intensities ($\approx 50$ m$\mu$A) to minimize any possible convection effects, as well as to avoid discharges in the chamber.

[4] A. Ghiorso and T. Sikkeland, Lawrence Radiation Laboratory (private communication).
[5] E. W. Valyocsik, Master's thesis, Lawrence Radiation Laboratory Report UCRL-8855, 1959 (unpublished).
[6] L. Bryde, N. O. Lassen, and N. O. Roy Poulsen, Kgl. Danske Videnskab. Selskab, Mat. Fys. Medd. 33, No. 8 (1962).

Under these conditions the plate voltage was not affected by the beam, and the ion current in the chamber was proportional to the beam intensity. The profile of the pulses of ion current in the chamber was essentially the same as those of the beam. Under typical experimental conditions, there were about $3\times10^9$ projectiles per beam pulse, or (assuming 30 eV per ion pair) about $5\times10^{14}$ ion pairs produced. This corresponds to an ion density in the direct beam of about $3\times10^{13}$ ions/ml, compared to about $10^{19}$ molecules/ml of gas. We actually collected about (2 to 10)$\times10^{12}$ positive ions (measured by the integrated current on the negative plate), and 3 to 10 times as many negative ions per beam burst. Presumably, the difference between positive and negative ion collection is due to electrons ejected from the target and window foils. Extensive recombination of the ionized gas molecules must take place, but 40 to 70% of the rare-earth recoils are collected on the negative plate. (The collection efficiency was determined by comparison of the number of recoils collected electrostatically with that from a separate monitor target placed just upstream from the target shown in Fig. 1.)

### B. Tests of the Method

One cannot be sure *a priori* of the relationship between the recoil range and the point at which a recoil is collected, and the horizontal distance from target to point of collection may differ from the projected recoil range. Therefore a variety of tests have been performed. The results of typical experiments are shown in Figs. 2 and 3. A Gaussian function (indicated by the straight lines on the probability plot) provides a good fit to most of the observed distribution. In most experiments a "short-range tail" is observed, which is not fit by the Gaussian plots. (This tail never contains more than 3% of the recoils collected; however, the magnitude and shape are not reproducible.)

If this tail is neglected, the range distributions can be represented by the median range $R_0$ and standard deviation $\sigma$ (or range straggling parameter $\rho=\sigma/R_0$) as determined from the Gaussian fit. Alternatively, the average range is given by

$$\langle R\rangle=\sum_i F_i d_i, \tag{1}$$

where $F_i$ is the fraction of the collected activity on the $i$th strip, and $d_i$ is the projected distance from the target to the center of this strip (increased by the stopping equivalent in $H_2$ of one-half the target thickness); the mean range fluctuation is given by

$$\langle\Delta R^2\rangle/\langle R\rangle^2=\sum_i F_i(d_i-\langle R\rangle)^2/\langle R\rangle^2. \tag{2}$$

As shown in Tables I and II, the difference between $R_0$ and $\langle R\rangle$ is negligible, and these two parameters are practically interchangeable. The difference between $\rho^2$ and $\langle\Delta R^2\rangle/\langle R\rangle^2$ depends on the magnitude of the short-range tail. This tail was essentially eliminated by a wide-angle collimator, which removed recoils at very large angles (position c in Fig. 1), as shown in Fig. 4. The collimator accepted all angles with appreciable cross sections as determined by angular-distribution measurements.[3] These facts and the inability to reproduce the shape of the tail lead us to believe that the tail is mainly of instrumental origin. Therefore we eliminate the tail from our analysis and use the Gaussian parameters $R_0$ and $\rho$. Standard deviations for a single

TABLE I. Results of some experimental tests.

| Expt. number | $E_b$ (MeV) | $p$ (in. Hg) | Field[a] (V/in.) | $R_0$ (in.) | $R_0$ (mg/cm²) | $\rho$ | $\langle R\rangle/R_0$ | $\langle\Delta R^2\rangle^{1/2}/\langle R\rangle\rho$ |
|---|---|---|---|---|---|---|---|---|
| | | | $Nd^{144}(C^{12},7n)Dy^{149}$ | | | | | |
| 1[b] | 113.0 | 8.05 | 2000/2 | 3.70 | 0.211 | 0.134 | 0.975 | 1.44 |
| 2[c] | 113.0 | 8.07 | 2000/2 | 3.62 | 0.209 | 0.131 | 0.983 | 1.33 |
| | | | $Ce^{140}(O^{16},7n)Dy^{149}$ | | | | | |
| 3[d] | 145.0 | 11.83 | 2000/2 | 3.99 | 0.336 | 0.096 | 0.999 | 1.03 |
| 4[d] | 145.0 | 11.76 | 1333/2 | 3.98 | 0.333 | 0.099 | 0.999 | 1.06 |
| 5[d] | 145.0 | 11.70 | 2000/3 | 4.07 | 0.339 | 0.106 | 1.000 | 1.08 |
| 6[d] | 145.9 | 7.78 | 2000/3 | 5.74 | 0.317 | 0.100 | 0.996 | 1.06 |
| 7[d] | 142.7 | 22.38 | 666/1 | 2.04 | 0.324 | 0.123 | 0.995 | 1.15 |
| 8[d] | 142.7 | 22.24 | 2000/3 | 2.01 | 0.317 | 0.178 | 0.950 | 1.54 |

[a] Potential difference divided by distance between plates.
[b] Target thickness of 80 μg/cm².
[c] Target thickness of 10 μg/cm².
[d] Target thickness of 32 μg/cm².

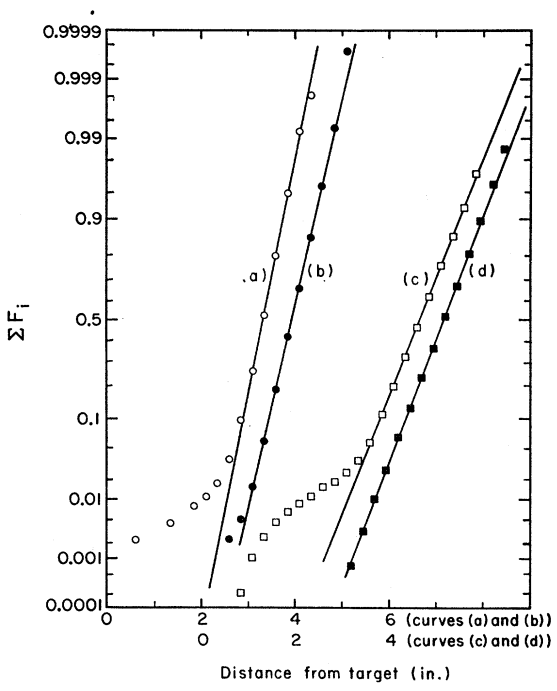


FIG. 4. Probability plots for the following range distributions: (a) $Ce^{140}(O^{16},7n)Dy^{149}$; $E_b=144.5$ MeV, $p=13.60$ in. Hg, normal collector position. (b) $Ce^{140}(O^{16},7n)Dy^{149}$; $E_b=145.0$ MeV, $p=11.83$ in. Hg, recessed collector position. (c) $Nd^{144}(C^{12},7n)Dy^{149}$; $E_b=109.3$ MeV, $p=6.09$ in. Hg, normal collector position. (d) $Nd^{144}(C^{12},7n)Dy^{149}$; $E_b=109.4$ MeV, $p=6.01$ in. Hg, recessed collector position. Plot (d) is displaced by 0.5 in. with respect to (c).

TABLE II. Stopping of Tb and Dy ions in hydrogen.

| $E_R$[a] (MeV) | $p$ (in. Hg) | $R_0$ (in.) | $R_0$ (mg/cm²) | $\rho$ | $\langle R\rangle/R_0$ | $\langle\Delta R^2\rangle^{1/2}/\langle R\rangle\rho$ | $F(R_0-\sigma)/F_G$ | $F(R_0-2\sigma)/F_G$ | $F(R_0+2\sigma)/F_G$ |
|---|---|---|---|---|---|---|---|---|---|
| 4.36(1) | 3.90 | 4.22 | 0.117 | 0.144 | 0.973 | 1.47 | 1.16 | 3.41 | 1.00 |
| 4.90(1) | 6.66 | 2.78 | 0.132 | 0.156 | 0.981 | 1.24 | 1.27 | 3.45 | 1.00 |
| 5.28(1) | 4.65 | 4.08 | 0.135 | 0.152 | 0.988 | 1.25 | 1.10 | 2.23 | 1.00 |
| 5.55(2) | 5.12 | 4.31 | 0.157 | 0.132 | 0.998 | 1.17 | 1.01 | 2.14 | 1.00 |
| 5.81(2) | 6.60 | 3.28 | 0.153 | 0.141 | 0.980 | 1.37 | 1.29 | 3.67 | 1.00 |
| 5.82(2) | 4.80 | 4.39 | 0.151 | 0.147 | 0.985 | 1.20 | 1.15 | 2.81 | 1.01 |
| 5.84(2) | 4.81 | 4.56 | 0.156 | 0.144 | 0.995 | 1.08 | 1.11 | 1.50 | 0.99 |
| 5.98(3) | 5.08 | 4.21 | 0.153 | 0.184 | 0.985 | 1.21 | 1.06 | 2.50 | 1.00 |
| 6.48(3) | 6.24 | 4.13 | 0.167 | 0.191 | 0.984 | 1.20 | 1.08 | 2.42 | 1.00 |
| 6.96(4) | 6.93 | 3.73 | 0.186 | 0.130 | 0.989 | 1.20 | 1.21 | 3.00 | 1.00 |
| 7.06(2) | 6.93 | 3.69 | 0.183 | 0.144 | 0.989 | 1.20 | 1.21 | 3.00 | 1.00 |
| 7.08(3) | 6.24 | 3.92 | 0.173 | 0.211 | 0.993 | 1.08 | 1.00 | 1.82 | 1.00 |
| 7.52(4) | 7.83 | 3.57 | 0.192 | 0.126 | 0.962 | 1.45 | 1.25 | 3.35 | 1.00 |
| 7.57(5) | 7.83 | 3.54 | 0.190 | 0.135 | 0.962 | 1.45 | 1.25 | 3.35 | 1.00 |
| 8.03(4) | 6.09 | 4.74 | 0.206 | 0.137 | 0.995 | 1.15 | 1.00 | 1.31 | 1.00 |
| 8.04(4) | 6.01 | 4.85 | 0.207 | 0.138 | 0.997 | 0.956 | 1.00 | 1.00 | 1.01 |
| 8.04(4) | 6.00 | 4.88 | 0.208 | 0.142 | 1.01 | 0.965 | 1.00 | 1.27 | 1.01 |
| 8.04(4) | 5.97 | 4.85 | 0.206 | 0.136 | 0.996 | 0.949 | 1.00 | 1.27 | 1.01 |
| 8.29(4) | 8.50 | 3.56 | 0.212 | 0.131 | 0.981 | 1.35 | 1.20 | 3.14 | 1.00 |
| 8.29(4) | 8.05 | 3.70 | 0.211 | 0.134 | 0.975 | 1.38 | 1.10 | 2.40 | 1.00 |
| 8.29(4) | 8.07 | 3.62 | 0.209 | 0.131 | 0.983 | 1.33 | 1.03 | 2.27 | 1.00 |
| 8.35(5) | 8.50 | 3.51 | 0.207 | 0.138 | 0.981 | 1.35 | 1.20 | 3.14 | 1.00 |
| 8.35(5) | 8.05 | 3.65 | 0.209 | 0.146 | 0.975 | 1.38 | 1.10 | 2.40 | 1.00 |
| 8.58(6) | 8.15 | 3.88 | 0.225 | 0.096 | 0.993 | 1.21 | 1.24 | 3.56 | 1.00 |
| 8.87(6) | 7.54 | 4.30 | 0.230 | 0.106 | 0.992 | 1.19 | 1.09 | 2.14 | 1.00 |
| 10.01(6) | 10.12 | 3.50 | 0.252 | 0.098 | 0.994 | 1.19 | 1.12 | 2.44 | 1.00 |
| 10.84(8) | 10.27 | 3.55 | 0.259 | 0.094 | 0.987 | 1.47 | 1.24 | 3.40 | 1.00 |
| 10.91(7) | 10.27 | 3.56 | 0.261 | 0.102 | 0.987 | 1.47 | 1.24 | 3.40 | 1.00 |
| 10.98(6) | 10.27 | 3.58 | 0.261 | 0.100 | 0.987 | 1.47 | 1.24 | 3.40 | 1.00 |
| 11.75(8) | 10.94 | 3.64 | 0.283 | 0.094 | 0.994 | 1.18 | 1.10 | 2.09 | 1.00 |
| 11.83(7) | 10.94 | 3.64 | 0.283 | 0.098 | 0.994 | 1.18 | 1.10 | 2.09 | 1.00 |
| 13.04(8) | 12.52 | 3.49 | 0.311 | 0.093 | 0.993 | 1.16 | 1.01 | 1.49 | 1.00 |
| 13.31(7) | 12.52 | 3.50 | 0.312 | 0.098 | 0.993 | 1.16 | 1.01 | 1.49 | 1.00 |
| 14.16(8) | 13.60 | 3.37 | 0.326 | 0.096 | 0.990 | 1.31 | 1.24 | 2.78 | 1.00 |
| 14.20(8) | 11.83 | 3.99 | 0.336 | 0.096 | 0.999 | 1.03 | 1.00 | 1.21 | 1.00 |
| 14.20(8) | 11.76 | 3.98 | 0.333 | 0.099 | 0.999 | 1.06 | 1.00 | 1.00 | 1.00 |
| 14.29(8) | 7.78 | 5.74 | 0.317 | 0.100 | 0.996 | 1.06 | 1.00 | 1.57 | 1.00 |
| 14.40(9) | 10.52 | 4.26 | 0.321 | 0.102 | 0.997 | 1.15 | 1.04 | 1.87 | 0.99 |
| 14.62(13) | 11.42 | 3.87 | 0.322 | 0.099 | 0.995 | 1.24 | 1.14 | 2.59 | 0.99 |
| 14.72(12) | 11.42 | 3.88 | 0.323 | 0.094 | 0.995 | 1.24 | 1.14 | 2.59 | 0.99 |
| 17.05(11) | 12.00 | 4.21 | 0.359 | 0.095 | 0.994 | 1.30 | 1.04 | 2.16 | 1.00 |
| 17.27(9) | 12.00 | 4.21 | 0.359 | 0.100 | 0.994 | 1.30 | 1.04 | 2.14 | 1.00 |
| 17.46(14) | 12.64 | 4.05 | 0.365 | 0.091 | 0.994 | 1.14 | 1.10 | 2.38 | 1.00 |
| 17.58(13) | 12.64 | 4.05 | 0.365 | 0.091 | 0.994 | 1.14 | 1.10 | 2.38 | 1.00 |
| 18.43(11) | 13.44 | 3.98 | 0.381 | 0.090 | 0.999 | 1.15 | 1.03 | 2.00 | 0.99 |
| 18.56(10) | 13.44 | 4.02 | 0.385 | 0.094 | 0.999 | 1.15 | 1.03 | 2.00 | 0.99 |
| 18.68(9) | 13.44 | 4.01 | 0.384 | 0.092 | 0.999 | 1.15 | 1.03 | 2.00 | 0.99 |
| 20.70(11) | 15.10 | 3.96 | 0.425 | 0.080 | 0.995 | 1.33 | 1.04 | 2.23 | 0.99 |
| 20.73(11) | 14.97 | 3.93 | 0.418 | 0.084 | 0.999 | 1.18 | 1.00 | 1.54 | 0.99 |
| 20.87(10) | 14.97 | 3.94 | 0.419 | 0.090 | 0.999 | 1.18 | 1.00 | 1.54 | 0.99 |
| 21.26(14) | 15.63 | 3.74 | 0.414 | 0.092 | 0.998 | 1.15 | 1.00 | 1.50 | 1.00 |

[a] The recoil energies were calculated by means of Eq. (6) for the following nuclear reactions:

(1) $Pr^{141}(C^{12},4n)Tb^{149g}$
(2) $Nd^{144}(C^{12},5n)Dy^{151}$
(3) $Nd^{146}(B^{11},8n)Tb^{149g}$
(4) $Nd^{144}(C^{12},7n)Dy^{149}$
(5) $Nd^{144}(C^{12},6n)Dy^{150}$
(6) $Ce^{140}(O^{16},5n)Dy^{151}$
(7) $Ce^{140}(O^{16},6n)Dy^{150}$
(8) $Ce^{140}(O^{16},7n)Dy^{149}$
(9) $Ba^{138}(Ne^{20},7n)Dy^{151}$
(10) $Ba^{138}(Ne^{20},8n)Dy^{150}$
(11) $Ba^{138}(Ne^{20},9n)Dy^{149}$
(12) $Ba^{136}(Ne^{20},5n)Dy^{151}$
(13) $Ba^{136}(Ne^{20},6n)Dy^{150}$
(14) $Ba^{136}(Ne^{20},7n)Dy^{149}$.

determination of $R_0$ and $\rho$ are about 2% and 5%, respectively.

The observed distributions of radioactivity may be affected by the following experimental factors: (a) scattering due to finite target thickness, (b) diffusion of recoil ions or atoms before collection, (c) drift due to convection currents, and (d) inhomogeneity of the electric field and its distortion by edge effects (primarily near the target itself). The field shape for a very similar arrangement has been discussed in some detail by Bryde, Lassen, and Poulsen.[6] The target mount is the only appreciable source of bending of the field lines in the forward or backward directions, and this effect is shown to be negligible for average ranges of $\approx 3$ to 6 in.

The magnitude of diffusion and convection effects is related to the diffusion coefficient ($D$) for Dy in $H_2$ and the average collection time $t$; $D$ varies inversely with pressure and can be estimated to be approximately

1 cm²/sec at 1/2 atm.[7] The drift velocity of the ions is given by

$$\bar{v}=DEq/kT, \tag{3}$$

where $E$ is the field strength, $q$ the ionic charge, $k$ Boltzmann's constant, and $T$ the absolute temperature. The mean-square displacement due to diffusion is given by

$$\langle X^2\rangle=Dt. \tag{4}$$

From these expressions we can conclude that if the recoil ions retain their positive charge until collection, the collection time $t$ is about $10^{-4}$ sec and the diffusion distance is about $10^{-2}$ cm. This would have essentially no effect on the initial range distribution. Significant diffusion could occur only if the recoils in the gas were neutralized for a time greater than $\approx 1/4$ sec. We have not measured the collection time directly, but we estimated its effect on the recoil distributions by varying field strength, gas pressure, and interplate distance. The variance $\sigma^2$ of the observed distribution is related to the collection time by the equations

$$\sigma^2=\sigma_r^2+\sigma_d^2 \quad \text{and} \quad \sigma_d^2=2Dt, \tag{5}$$

in which $\sigma_r^2$ and $\sigma_d^2$ denote, respectively, the contributions of the range distribution and of diffusion to the observed variance. Table I shows the result of several illustrative experiments. The first four columns give the experiment number, beam energy, gas pressure, and potential difference and distance between the plates; the last columns give the experimental results. Comparison of experiments 1 and 2 indicates that the Gaussian parameters $R_0$ and $\rho$ do not depend on target thickness. Also, it is clear from the same experiments that the short-range tail can be only partially attributed to scattering in the target layer.

Comparison of experiments 3 and 4 shows that the values of $R_0$ and $\rho$ (for ranges of $\approx 4$ in.) are independent of the field strength. Similarly, experiments 4 and 5 indicate insensitivity to distance between the plates for comparable field strengths. And, most revealing of all, experiments 5 and 6 show that $R_0$ and $\rho$ are insensitive to pressure. These experiments vary the time required to collect an ion (average path length divided by average velocity) by a factor of approximately 9/4. If diffusion played a leading role in determining the measured distribution, then the standard deviation $\sigma(\sigma=R_0\rho)$ would increase with increasing collection time [see Eq. (5)]. This is certainly not the case. We conclude that for average ranges of $\approx 4$ to 6 in. the standard deviation from diffusion is negligible ($<0.1$ in.).

Ranges of about 2 in. do exhibit an instrumental broadening, as shown by experiments 7 and 8. Although the standard deviation observed in experiment 7 is only 0.25 in., the $\rho$ value is $\approx 25\%$ greater than that found in experiments 3 to 6. We attribute the additional broadening ($\approx 0.05$ in.) to distortion of the electric field in the region near the target mount. The comparison of experiments 7 and 8 shows that the distribution (for $R_0\approx 2$ in.) is broadened by an increased distance between the plates. Even though an instrumental broadening was observed in experiment 7, the small standard deviation of about 1/4 in. provides additional evidence that diffusion broadening is negligible if the average range is about 4 in. ($\sigma\approx 0.4$ in. in this case, and a 20% diffusion effect would result in a standard deviation due to diffusion $\sigma_d\approx 0.24$ in., which is incompatible with experiment 7).

The picture of the collection process that emerges from these experiments is as follows. A recoiling ion is ejected from the thin target layer and brought to an epithermal energy in about $10^{-7}$ sec. Most (40 to 70%) of the ions either retain their positive charge for the $10^{-4}$ sec required for collection or are reionized positively by the ionizing radiation during the beam pulse of $\approx 3$ msec. The collection of neutral atoms is negligible as shown by inefficient collection on the positive plate. Diffusion of the recoils leads to a root-mean-square horizontal displacement of less than 0.1 in. This sets an upper limit of $\approx 0.05$ sec, or about 2 beam bursts for collection. The width of the range distribution, as characterized by $\rho$, is determined by the initial distribution of recoil velocities and by the statistical nature of the stopping process. It is not affected by target thickness or by instrumental sources.

## III. RESULTS AND DISCUSSION

The results of the Tb and Dy stopping experiments are summarized in Table II. The initial energy of the Hilac beam was assumed to be 10.38 MeV/amu, and the range-energy curves of Northcliffe were used to calculate the energy losses in the window, degraders, and target backing.[8] A mass stopping-power ratio of 3.3 (mg $H_2$/mg Al) was assumed for estimating the energy loss in the gas between the window and the target. The error introduced by this assumption is negligible. The average recoil energies $E_R$ were calculated from the bombarding energy $E_b$ and from the mass numbers $A$ of the bombarding, target, and recoil atoms designated, respectively, by the subscripts $b$, $T$, and $R$.

$$E_R=E_bA_bA_R/(A_b+A_T)^2; \tag{6}$$

total momentum transfer was assumed.[1,3]

The range distributions are characterized by the Gaussian parameters $R_0$ (in units of length and mass per unit area) and $\rho$. The median range and the average range [Eq. (1)] never differ by more than a few percent (column 6). The difference between $\rho$ and the mean range fluctuation [Eq. (2)] is more significant (column 7). This difference is clearly correlated with the magni-

[7] W. Jost, *Diffusion in Solids, Liquids, Gases* (Academic Press Inc., New York, 1952).

[8] L. C. Northcliffe, Phys. Rev. **120**, 1744 (1960).

TABLE III. Values of the exponent $N$ in $R_0=kV_L{}^N$.

| Average recoil energy, $E_R$ (MeV) | $N$ |
|---|---|
| 6 | 1.80 |
| 9 | 1.71 |
| 12 | 1.61 |
| 15 | 1.50 |
| 18 | 1.38 |
| 21 | 1.26 |

tude of the short-range tail discussed above, as shown in columns 8 through 10, which give the ratios of the cumulative fractional activities $F$ at $R_0-\sigma$, $R_0-2\sigma$, and $R_0+2\sigma$ to the corresponding quantities $F_G$ obtained from the Gaussian fits. As stated above, most of this tail is due to instrumental effects; therefore, we use the Gaussian parameters for our analysis. This procedure is supported by Monte Carlo calculations of the range distribution caused by the initial velocity spread of the recoiling ions, according to which the distribution can be very closely approximated by a Gaussian function.[9]

A range-energy plot of the results of Table II is given in Ref. 10. For analyzing the data in terms of the initial velocity distribution of the recoiling atoms, it is convenient to represent the range-energy relationship by the empirical form

$$R_0=kV_L{}^N, \tag{7}$$

in which $V_L$ denotes the average recoil velocity in laboratory-system coordinates, and $k$ and $N$ are constants. In practice, it is found that the exponent $N$ varies slowly with energy, i.e., Eq. (7) gives an adequate representation of restricted regions of the range-energy curve. Values of $N$ as a function of the mean recoil energy were obtained by a least-squares fit of the data to a second-degree polynomial $R_0=a_0+a_1E_R+a_2E_R{}^2$, followed by logarithmic differentiation of this polynomial. The experiments with an $O^{16}$ beam resulted in ranges systematically higher by a few percent than those obtained with $C^{12}$ or $Ne^{20}$ beams. In order to minimize errors due to such systematic differences, overlapping regions of the curve were fitted separately, and the values of $N$ thus obtained were averaged. The results are summarized in Table III. In the middle portion of the curve ($E_R$ of 6 to 15 MeV) the values are quite accurate, the probable error being $\pm5\%$. Towards both ends of the curve the uncertainties increase to about $\pm10\%$.

As pointed out earlier, both the recoil-velocity distribution and the stopping process are expected to contribute to the measured range straggling, i.e.,

$$\rho^2=\rho_n{}^2+\rho_s{}^2, \tag{8}$$

where the subscripts $n$ and $s$ denote, respectively, the contributions of the nuclear and stopping processes. In Ref. 10, we make a detailed comparison of theoretical predictions with stopping measurements of Dy recoils in a series of gases from He to Xe. In general, the range straggling is in agreement with theoretical predictions, provided the single parameter of the theory is adjusted in accordance with the range-energy data. This result for heavier gases justifies the use of theoretical values of $\rho_s{}^2$ in $H_2$ to correct for the stopping effect. This correction is actually quite small, as the calculated values of $\rho_s{}^2$ are only about 10% of the observed values of $\rho^2$.

For isotropic neutron emission, the range straggling parameter $\rho_n$ is related to the average total c.m. energy $T_n$ of the emitted neutrons by the equation[3]

$$T_n=\frac{3E_bA_b(A_b+A_T+A_R)^2\rho_n{}^2}{4N^2(A_b+A_T)^2}. \tag{9}$$

A similar relation connects the mean-square recoil angle $\langle\theta_L{}^2\rangle$ (in the laboratory system) to $T_n$:

$$T_n=\frac{3E_bA_b(A_b+A_T+A_R)^2\langle\theta_L{}^2\rangle}{8(A_b+A_T)^2}. \tag{10}$$

If the neutron emission is not isotropic, these relations are no longer valid. For a given total neutron energy $T_n$, preferential emission in the forward-backward direction gives rise to a broadened velocity distribution along the beam, i.e., enhanced range straggling. At the same time, the recoil-velocity distribution perpendicular to the beam is narrowed, and the value of $\langle\theta_L{}^2\rangle$ is reduced. The opposite effect would be observed if the neutron emission were peaked at 90 deg.

Thus, the parameter $\alpha$, defined as

$$\alpha=2\rho_n{}^2/N^2\langle\theta_L{}^2\rangle \tag{11}$$

is a measure of the anisotropy of the neutron emission ($\alpha=1$ for isotropic, $\alpha>1$ for forward-backward peaking, and $\alpha<1$ for 90 deg peaking). The exact calculation of $T_n$ for $\alpha\neq1$ is difficult, since in this case both the recoil probability $W$ and recoil velocity $V$ are functions of the c.m. angle $\theta$.

If we ignore the dependence of $V$ on $\theta$, and represent the angular distribution in the c.m. system by

$$W(\theta)=a+b\cos^2\theta, \tag{12}$$

we obtain the following approximate relationships for the average total neutron energy:

$$\begin{aligned}T_n&=\frac{3E_bA_b(A_b+A_T+A_R)^2\langle\theta_L{}^2\rangle}{8(A_b+A_T)^2}\times\frac{2+\alpha}{3}\\&=\frac{3E_bA_b(A_b+A_T+A_R)^2\rho_n{}^2}{4N^2(A_b+A_T)^2}\times\frac{2+\alpha}{3\alpha},\end{aligned} \tag{13}$$

[9] L. L. Altman, Lawrence Radiation Laboratory (private communication).

[10] J. Gilat and J. M. Alexander, following paper, Phys. Rev. **136**, B1298 (1964).

and for the anisotropy, we obtain

$$\frac{d\sigma(0°)-d\sigma(90°)}{d\sigma(90°)}=\frac{b}{a}=\frac{5(\alpha-1)}{3-\alpha}. \tag{14}$$

The average total photon energy is given by

$$T_\gamma=E_a-T_n, \tag{15}$$

where $E_a=E_{c.m.}+Q$ is the total available excitation energy. The values of $\alpha$ measured in this work have uncertainties of $\approx 15\%$, which correspond to errors of 60% or more in the anisotropy parameter $b/a$, as determined by Eq. (14). Therefore, anisotropies deduced from our measurements of $\rho$ and $\langle\theta_L^2\rangle^{1/2}$ can be used only qualitatively. Nevertheless, the total neutron energy $T_n$ as given by Eq. (13) is quite insensitive to uncertainties in the value of $\alpha$, and the error introduced by a 15% uncertainty in $\alpha$ will be 5 to 9%.

The anisotropy is determined by the correlation between the angular momentum **J** of the compound nucleus and the orbital angular momentum **l** of an evaporated neutron. If **J** is perpendicular to the beam and if **l** and **J** are completely aligned, then the angular distribution of each neutron is expected to be proportional to $1/\sin\theta$. If **J** and **l** are completely uncorrelated (or decoupled), then the angular distribution of each neutron is isotropic and, of course, the angular distribution of the final nucleus $[W(\theta)]$ is isotropic. For the highly excited Dy compound systems $J\gg l$, and we expect the situation to be closer to the latter limiting case.

To illustrate this we shall use the approximate relationship derived by Ericson and Strutinski[11] for a level density proportional to $\exp[-J^2/2\mathcal{I}T]$

$$\frac{b}{a}=\frac{\hbar^4\langle J^2\rangle\langle l^2\rangle}{4\mathcal{I}^2T^2}, \tag{16}$$

where $\mathcal{I}$ and $T$ are, respectively, the moment of inertia and the nuclear temperature of the residual nucleus, and $\hbar$ is Planck's constant. At reasonably high excitation energies, the moment of inertia is expected to be essentially equal to that of a rigid body. For neutron emission from a rigid sphere of radius $1.2A^{1/3}$ F, Eq. (16) yields a value of $\approx 0.2$ for $b/a$, if $\langle J^2\rangle=10^3$, $\langle l^2\rangle=10$, and $T=2$ MeV.

It is quite likely that in neutron emission the removal of excitation energy is much more rapid than the removal of angular momentum.[12] If there is a scarcity of low-lying, high spin states, then Eq. (16) is not valid for the last emitted neutron (or possibly neutrons), and the angular momentum of this last neutron may be strongly aligned antiparallel to the angular momentum of the emitting nucleus. The resulting angular distribution may approach the classical limit of $1/\sin\theta$. Detailed knowledge of the level density would be required for a quantitative prediction of this effect. However, on the basis of the above considerations one would expect the angular distribution of the final Dy product to be characterized by $b/a\gtrsim 1$ or $\alpha\gtrsim 1.3$.

This prediction is verified by the values of $\alpha$ in Table IV for the reactions $Nd^{144}(C^{12},xn)Dy^{156-x}$ and $Ce^{140}(O^{16},xn)Dy^{156-x}$, with $x=5$, 6, or 7. These values of $\alpha$ are all less than 1.4 and no significant correction is required for the corresponding values of $T_n$ and $T_\gamma$ in Ref. 3. In Table IV the values of $\alpha$ were obtained from values of $N$ taken from Table III and values of $\langle\theta_L^2\rangle$ from Ref. 3. Within the framework of the analysis leading to Eq. (13), the values of $T_n$ for the $B^{11}$, $C^{12}$, and $O^{16}$ reactions are uncertain by $\approx\pm 15\%$ and the relative values by about $\pm 10\%$. For the $Ce^{140}(O^{16},7n)$-$Dy^{149}$ reaction, the average value of $\alpha$ actually drops slightly below 1. This provides an *a posteriori* justification of the assumptions used to derive $\rho_n$ from the measured $\rho$, since any further corrections would lead to neutron emission peaked at 90 deg, in marked contradiction with theory.

For the very similar reactions of $Ne^{20}$ with $Ba^{136}$ and $Ba^{138}$, the values of $\alpha$ appear to be significantly higher (1.2 to 1.7). However, the values of $\langle\theta_L^2\rangle$ used are not based on direct measurements but were estimated from Eq. (10) and Fig. 5 of Ref. 3. The assumption is made that the general trends obtained with other reactions can be extrapolated to $Ne^{20}$ beams and eight or nine evaporated neutrons.[13] Therefore these values are less certain than those obtained from $C^{12}$ and $O^{16}$ reactions. Furthermore, for the $Ne^{20}$ reactions, $N$ is derived from the upper portion of the range-energy curve; it is therefore subject to considerably larger errors. Also, the relative importance of small diffusion effects increases with decreasing $\rho$, and the energy spread of the degraded beam (larger for the more highly ionizing $Ne^{20}$ than for either $O^{16}$ or $C^{12}$) may also begin to affect these quite narrow distributions. Thus, the apparent anisotropy could be due to systematic errors in the experimental values of $\rho^2$. In view of these uncertainties we have not calculated $T_n$ from the $Ne^{20}$ results.

A surprising result of this study is the large anisotropy indicated for the reactions $Pr^{141}(C^{12},4n)Tb^{149g}$ and $Nd^{146}(B^{11},8n)Tb^{149g}$. Reactions of this type, which lead to the low-spin member of an isomeric pair, are expected to proceed selectively from compound states of lower-than-average spin. Previously reported cross-section data imply that the particular reactions under study

[11] T. Ericson and V. Strutinski, Nucl. Phys. 8, 284 (1958).

[12] Torleif Ericson, *The Statistical Model and Nuclear Level Densities in Advances in Physics*, edited by N. F. Mott (Taylor and Francis, Ltd., London, 1960), Vol. 9, p. 425.

[13] A few angular distributions of recoils from the $Ba^{136}(Ne^{20},7n)$-$Dy^{149}$ and $Ba^{138}(Ne^{20},9n)Dy^{149}$ were measured and found to be consistent with this assumption; however, due to experimental difficulties, these measurements had to be carried out with fairly thick targets, and were not exactly comparable with those of Ref. 3. Therefore, we cannot consider the assumption to be verified.

TABLE IV. Comparison of range distributions with angular distributions.

| $E_b$ (MeV) | $\rho_n^2$ | $\alpha=2\rho_n^2/N^2\langle\theta_L^2\rangle$ |
|---|---|---|
| $Pr^{141}(C^{12},4n)Tb^{149g}$ | | |
| 57.1 | 0.0188 | $>1.8_0$ |
| 64.1 | 0.0225 | $1.9_1$ |
| 69.1 | 0.0214 | $1.6_8$ |
| $Nd^{146}(B^{11},8n)Tb^{149g}$ | | |
| 89.9 | 0.0323 | $1.9_5$ |
| 97.5 | 0.0350 | $1.6_9$ |
| 106.5 | 0.0431 | $1.6_4$ |
| $Nd^{144}(C^{12},5n)Dy^{151}$ | | |
| 74.5 | 0.0157 | $1.1_6$ |
| 78.2[a] | 0.0191[a] | $1.3_9$[a] |
| 94.8 | 0.0193 | $1.3_5$ |
| $Nd^{144}(C^{12},6n)Dy^{150}$ | | |
| 102.4 | 0.0169 | $1.1_2$ |
| 113.0[b] | 0.0189[b] | $1.1_7$[b] |
| $Nd^{144}(C^{12},7n)Dy^{149}$ | | |
| 94.8 | 0.0155 | $1.1_3$ |
| 102.4 | 0.0146 | $1.0_4$ |
| 109.4[c] | 0.0178[c] | $1.1_9$[c] |
| 113.0[a] | 0.0162[a] | $1.0_3$[a] |
| $Ce^{140}(O^{16},5n)Dy^{151}$ | | |
| 86.4 | 0.0080 | $1.0_6$ |
| 89.3 | 0.0100 | $1.2_9$ |
| 100.8 | 0.0085 | $1.0_9$ |
| 110.6 | 0.0090 | $1.0_6$ |
| $Ce^{140}(O^{16},6n)Dy^{150}$ | | |
| 110.6 | 0.0094 | $1.1_0$ |
| 120.0 | 0.0087 | $0.9_5$ |
| 133.1 | 0.0087 | $1.0_3$ |
| $Ce^{140}(O^{16},7n)Dy^{149}$ | | |
| 110.6 | 0.0088 | $0.9_3$ |
| 120.0 | 0.0079 | $0.9_0$ |
| 133.1 | 0.0078 | $0.9_0$ |
| 145.0[c] | 0.0087[c] | $1.0_2$[c] |
| $Ba^{136}(Ne^{20},5n)Dy^{151}$ | | |
| 118.6 | 0.0080 | $(1.5_3)$[d] |
| $Ba^{136}(Ne^{20},6n)Dy^{150}$ | | |
| 118.6 | 0.0090 | $(1.6_7)$[d] |
| 142.6 | 0.0076 | $(1.4_2)$[d] |
| $Ba^{136}(Ne^{20},7n)Dy^{149}$ | | |
| 142.6 | 0.0076 | $(1.4_1)$[d] |
| 173.6 | 0.0079 | $(1.4_8)$[d] |
| $Ba^{138}(Ne^{20},7n)Dy^{151}$ | | |
| 119.0 | 0.0096 | $(1.6_6)$[d] |
| 142.6 | 0.0093 | $(1.6_4)$[d] |
| 154.4 | 0.0078 | $(1.4_1)$[d] |
| $Ba^{138}(Ne^{20},8n)Dy^{150}$ | | |
| 154.4 | 0.0082 | $(1.4_7)$[d] |
| 173.6 | 0.0075 | $(1.4_1)$[d] |
| $Ba^{138}(Ne^{20},9n)Dy^{149}$ | | |
| 142.8 | 0.0084 | $(1.4_4)$[d] |
| 154.4 | 0.0075 | $(1.3_6)$[d] |
| 173.5[b] | 0.0062[b] | $(1.2_0)$[d] |

[a] Average of three experiments.
[b] Average of two experiments.
[c] Average of four experiments.
[d] Based on extrapolated values of $\langle\theta_L^2\rangle$.

select compound states of $\langle J\rangle<7.5$.[14] In order to account for the observed anisotropy, these reactions must select the rare neutron-evaporation chains in which all the orbital angular-momentum vectors are essentially antiparallel to that of the compound system. For this case of strong correlation, the angular distribution of the neutrons is given classically as $W(\theta)\propto 1/\sin\theta$, which corresponds to $\alpha=2$, and the experimental values are very close to this value.[15]

At first glance the large anisotropies implied by this work are difficult to reconcile with the argument for the compound systems of low spin presented in Ref. 14. However, it is certainly possible that the production of $Tb^{149g}$ proceeds through compound nuclei of lower than average spin and still gives rise to much higher than average neutron anisotropies. If a sizable fraction of the evaporation chains is accompanied by appreciable angular-momentum removal ($\Delta J>2x$), large anisotropy would result. Such a situation could obtain even for a collection of compound nuclei with average spin of about 7.5, provided the collection contains a sufficient fraction of all compound nuclei to account for the observed cross section. (This would correspond to a rather long tail on curve $B$ in Fig. 3 of Ref. 14.) Thus it would appear that the low-spin product $Tb^{149g}$ provides a twofold selection of reactions. (a) First it selects reactions involving low angular momenta as inferred from the cross sections in Ref. 14. (b) Second it selects those particular neutron-emission chains which are very effective in removing angular momentum as inferred from the strong forward-backward peaking of the neutron angular distribution.

Values of $b/a$, $T_n$, and $T_\gamma$ for the two reactions [obtained from Eqs. (13), (14), and (15)], together with their respective errors (from experimental sources only), are tabulated in Table V. $Q$ values were obtained from Seeger's nuclear-mass tables.[16] Table V constitutes a substantial correction to the previously reported energetics of these reactions.[3] The previous work showed that in $Tb^{149g}$ reactions values of $T_\gamma$ vary only slowly with bombarding energy and are never greater than 12 MeV. Values of $T_\gamma$ in Dy reactions increase very rapidly with bombarding energy and in some cases exceed 30 MeV. The differences between these reactions are further accentuated by this study. The values in Table V are only approximate because Eqs. (13) and (14) ignore the variation of $V$ with $\theta$ which must exist

[14] J. M. Alexander and G. N. Simonoff, Phys. Rev. **130**, 2383 (1963).

[15] For $W(\theta)\propto 1/\sin\theta$, Eq. (13) becomes

$$T_n=\frac{E_bA_b(A_T+A_b+A_R)^2}{2(A_b+A_T)^2}\langle\theta_L^2\rangle$$

$$=\frac{E_bA_b(A_T+A_b+A_R)^2\rho_n^2}{2(A_b+A_T)^2N^2}.$$

Although this equation is derived from a different angular distribution $W(\theta)$ than that used for Eq. (13), it yields the same neutron energy $T_n$ as that obtained from Eq. (13) with $\alpha=2$. Therefore, our measurements cannot distinguish between the forward-backward peaking associated with $W(\theta)=a+b\cos^2\theta$ with $b/a=5.0$ (corresponding to $\alpha=2$), and the very strong peaking associated with the $1/\sin\theta$ distribution.

[16] P. A. Seeger, Nucl. Phys. **25**, 1 (1961).

TABLE V. Approximate anisotropy and average energies for reactions leading to $Tb^{149g}$.

| $E_b$ (MeV) | $E_{c.m.}+Q$ (MeV) | $\frac{d\sigma(0°)-d\sigma(90°)}{d\sigma(90°)}$ | $T_n$ (MeV) | $T_\gamma$ (MeV) |
|---|---|---|---|---|
| $Pr^{141}(C^{12},4n)Tb^{149g}$ | | | | |
| 57.1 | 5.6 | >3.3 | 7.7±1.2 | −2.1±1.2 |
| 64.1 | 12.1 | 4.2 | 10.3±1.5 | 1.8±1.5 |
| 69.1 | 16.7 | 2.6 | 11.5±1.7 | 5.2±1.7 |
| $Nd^{149}(B^{11},8n)Tb^{149g}$ | | | | |
| 89.9 | 17.5 | 4.5 | 19.0±2.9 | −2.5±2.9 |
| 97.5 | 24.6 | 2.6 | 24.3±3.7 | 0.3±3.7 |
| 106.5 | 32.9 | 2.4 | 34.0±5.1 | −1.1±5.1 |

for large anisotropies. These values are useful only to show that (within this analysis) very little energy is left for gamma de-excitation to this low-spin ground state of $Tb^{149}$. (In the absence of a kinematic analysis which includes the dependence of $V$ on $\theta$, a safe attitude would be that the values of $T_\gamma$ for these reactions are between zero and those values reported in Ref. 3.) If the angular distributions are essentially symmetric about 90 deg as concluded indirectly in Ref. 1, then almost all the available excitation energy is taken up by the neutrons, and the total photon energies are very small. Normally, as in the Dy reactions studied, the photons play an important role in the deexcitation of the compound system, presumably in the removal of angular momentum. Since in this case an unusually large portion of the angular momentum is taken away by the neutrons, the nuclei can de-excite without appreciable $\gamma$ emission.

## IV. SUMMARY

This paper concludes a series of experimental studies of the energetics of neutron and photon emission in the reactions ($C^{12}$ or $O^{16}$)+($Nd^{144}$ or $Ce^{140}$) → $Dy^{156*}$ → 5, 6, or $7n+Dy^{151,150,\text{ or }149}$, $C^{12}+Pr^{141}$ → $Tb^{153*}$ → $Tb^{149g}+4n$, and $B^{11}+Nd^{146}$ → $Tb^{157*}$ → $Tb^{149g}+8n$. Cross sections,[2,14] angular distributions,[3] average ranges,[1] and range dispersions have been measured. Within the framework of our analysis we reach the following conclusions: The average range measurements are consistent with neutron emission essentially symmetric about 90° in the c.m. system. (This indication can be subjected to stringent tests by independent range-energy studies.) Measurements of angular and range distributions lead to the determination of the average total neutron and photon energies ($T_n$ and $T_\gamma$). For reactions leading to the $Dy^{156*}$ compound system, neutron emission is approximately isotropic and the average total photon energy is a rapidly increasing function of excitation energy. In the production of $Tb^{149g}$ (low spin) from Tb compound systems, neutron emission is strongly peaked forward and backward, and very little energy is dissipated by photons.

These results provide a body of data for delimitation of nuclear-level density at high energy and angular momentum. However, a more refined calculation of nuclear evaporation than has been performed to date would be required for this purpose.

## ACKNOWLEDGMENT

We would like to thank the Hilac operating crew for their help in the experiments.